Uptake Kinetics of ^{99m}Tc-MAG$_3$-Antisense Oligonucleotide to PCNA and Effect on Gene Expression in Vascular Smooth Muscle Cells

Yan-Rong Zhang, PhD; Yong-Xue Zhang, MD; Wei Cao, PhD; and Xiao-Li Lan, PhD

Department of Nuclear Medicine, Union Hospital of Tongji Medical College, Huazhong University of Science and Technology, Wuhan, China

To investigate the feasibility of in vivo imaging study of atherosclerotic plaque and restenosis using antisense probe, we evaluated the uptake kinetics of radiolabeled oligonucleotides to the messenger RNA (mRNA) of proliferating cell nucleus antigen (PCNA) in vascular smooth muscle cells (VSMCs) and the effect on gene expression. **Methods:** The antisense oligonucleotide to PCNA was radiolabeled with ^{99m}Tc through bifunctional chelator mercaptoacetyltriglycine (MAG$_3$). The labeling efficiency was assessed by Sephadex G25 chromatography. The radiochemical purity, in vitro stability, and ability of the labeled antisense oligonucleotide to hybridize to its complement were analyzed by Sep-Pak C18 column chromatography. The uptake kinetics of ^{99m}Tc-labeled antisense oligonucleotide and sense oligonucleotide were studied in VSMCs in log and plateau phases. To study whether the antisense probe can hybridize to a respective sequence on the whole PCNA mRNA strand after radiolabeling, we performed reverse-transcriptase polymerase chain reaction to assay the PCNA mRNA level after the VSMCs had been incubated with the ^{99m}Tc-labeled antisense oligonucleotide and sense oligonucleotide. **Results:** The labeling efficiency of ^{99m}Tc-MAG$_3$-antisense oligonucleotide was 60.1% ($n = 5$), the specific activity was 1,960 kBq/μg, and the radiochemical purity was more than 95% after purification. ^{99m}Tc-MAG$_3$-antisense oligonucleotide was stable in vitro and retained the ability to hybridize with its complementary chain. Antisense oligonucleotide showed significantly higher accumulation than sense oligonucleotide in log phase, with peak values of 15.2% ± 0.58% and 5.6% ± 0.42%, respectively ($P < 0.05$). No significant difference was found between uptake of antisense oligonucleotide and uptake of sense oligonucleotide in plateau phase ($P > 0.05$), but higher accumulation of antisense oligonucleotide was found in log phase than in plateau phase ($P < 0.05$). The retention rate of antisense oligonucleotide in log phase was much higher than that of sense oligonucleotide (79.6% ± 0.96% vs. 59.8% ± 0.75%, $P < 0.05$) at 240 min. The 2 probes did not significantly differ in plateau phase ($P > 0.05$). The efflux of antisense oligonucleotide was obviously slower in log phase than in plateau phase ($P < 0.05$). Compared with ^{99m}Tc-MAG$_3$-sense oligonucleotide, ^{99m}Tc-MAG$_3$-antisense oligonucleotide could inhibit the expression of PCNA mRNA significantly. **Conclusion:** This in vitro study in VSMCs provided evidence that the ^{99m}Tc-labeled antisense oligonucleotide to PCNA can be used for in vivo imaging of atherosclerotic plaque and restenosis in further study.

Key Words: atherosclerotic plaque; restenosis; antisense oligonucleotide; proliferating cell nucleus antigen; vascular smooth muscle cells

J Nucl Med 2005; 46:1052–1058

Antisense technology is a pharmacy engineering approach developed within the last 20 y. Based on the Watson–Crick principle, it uses oligonucleotide strands that hybridize with specific sequences on candidate DNAs or messenger RNAs (mRNAs), thereby regulating the expression of the target gene at the level of replication, transcription, splicing, transportation, or translation. The research on antisense pharmaceuticals began in 1978, when Zamecnik (*1*) synthesized a 13mer-antisense oligodeoxyribonucleotide matching the mRNA of the Rous sarcoma virus to inhibit proliferation of the virus. With the rapid development of biotechnology, especially the Human Genome Project, research on antisense pharmaceuticals has generated increasing interest. Currently, antisense chemotherapy has proven to be effective in the treatment of cancer and viral inflammation (*2–5*).

Blood vessels are prime candidates for gene therapy because of novel percutaneous, catheter-based treatment methods. Some cardiovascular diseases such as atherosclerosis, cardiac allograft atherosclerosis, and restenosis share a characteristic of tumors: the abnormal proliferation of cells. The arteriopathy of both atherosclerosis and restenosis is characterized by a thickened intima comprising proliferative vascular smooth muscle cells (VSMCs). Some oncogenes (c-*myb*, c-*myc,* and c-*fos*) and cell cycle proteins (proliferating cell nucleus antigen [PCNA] and cell cycle-dependent kinase 2) that are highly expressed in malignant tumor tissue have also been found to be activated and highly expressed in the abnormally proliferating VSMCs in the early phase of arteriopathy. Gene therapy strategies aimed at inhibiting VSMC proliferation by using the antisense oli-

Received Aug. 1, 2004; revision accepted Mar. 7, 2005.

For correspondence or reprints contact: Yong-Xue Zhang, BS, Jiefang Dadao 1277, Hankou, Wuhan 430022, Hubei, China.

E-mail: Zhyx1229@163.com

gonucleotide of the oncogene and cell cycle protein have been shown to be effective in retarding the development of intima disease (*6–11*).

More recently, antisense oligonucleotides in nuclear medicine imaging, especially in tumor targeting, have been studied and found promising (*12–17*). However, only a few studies have focused on the gene imaging of cardiovascular diseases such as atherosclerotic plaque and restenosis using nuclear medicine imaging (*18*). For this reason, we studied an 18mer antisense oligonucleotide targeted to mRNA of PCNA, which is highly expressed in the early phase of atherosclerotic plaque and restenosis in the abnormally proliferative smooth muscle cells. The antisense oligonucleotide is complementary to the 5′ initiation codon regions of the respective mRNA, which has shown a sequence-specific effect in previous studies (*10*). In this study, we looked at the properties of the ^{99m}Tc-radiolabeled antisense probe by modifying the strands chemically and at the uptake and efflux of the radiolabeled DNA and PCNA mRNA expression in VSMCs after incubation with antisense probe.

MATERIALS AND METHODS

Two single strands of 18-base DNA sequences were purchased as uniform phosphorothioates (Sangon Biotech) for this study. The base sequences were 5′-GAT-CAG-GCG-TGC-CTC-AAA-3′ (antisense) and 5′-TTT-GAG-GCA-CGC-CTG-ATC-3 (sense). Each DNA had a primary amine on the 5′ end attached through a 6-carbon alkyl linker. The amine was designed for covalent conjugation with the chelator, mercaptoacetyltriglycine (MAG_3). The molecular weight of each chain was about 6.0 kDa. MAG_3 for conjugation was *N*-hydroxysuccinimide ester, donated by Donald J. Hnatowich (University of Massachusetts Medical School). The DNAs were generally handled under sterile conditions, as all solutions were sterilized by terminal filtration through a 0.22-μm filter and all pipette tips and tubes were sterilized by autoclaving. ^{99m}Tc was obtained from a ^{99}Mo–^{99m}Tc radionuclide generator (China Institute of Atomic Energy).

Oligonucleotide Conjugation and Radiolabeling

DNA conjugation and radiolabeling were by the methods of Winnard et al. (*19*) and Zhang et al. (*20*). The DNA was dissolved in a sterile bicarbonate buffer so that the final concentrations were DNA, 2 mg/mL; $NaHCO_3$, 0.25 mol/L; NaCl, 1 mol/L; and 1 mmol/L ethylenediaminetetraacetic acid (EDTA) at pH 8.5. A fresh 10 mg/mL solution of MAG_3 in dry *N,N*-dimethylformamide was added dropwise with agitation to reach a final chelator-to-DNA molar ratio of 15:1. The reaction mixture was then incubated at room temperature for 60 min before purification on a 0.7 × 28 cm Sephadex G25 column (Pharmacia) with saline as eluent. The peak fractions were collected and quantitated by the Gene Quant RNA/DNA Calculator (Amersham Pharmacia Biotech) at 260 nm (optical density, 33 μg/mL), dispensed at 10 μg per vial, lyophilized, and stored at −20°C for future use.

A fresh 50 mg/mL solution of sodium tartrate and a 1 mg/mL solution of $SnCl_2{\cdot}2H_2O$ were prepared just before use. Ten micrograms of conjugated and purified DNA were dissolved in 33 μL of ammonium acetate buffer (0.25 mol/L, pH 5.2). To the solution of coupled DNA was added an aliquot from a 50 mg/mL solution of sodium tartrate in sodium bicarbonate, 0.5 mol/L; ammonium acetate, 0.25 mol/L; and ammonium hydroxide, 0.175 mol/L, at pH 9.2 (for a labeling pH of 7.6), such that the final tartrate concentration was 7 μg/μL. After the addition of 19 MBq of ^{99m}Tc-pertechnetate generator eluent, 1 μL of a fresh solution of $SnCl_2{\cdot}2H_2O$ (1 mg/mL in HCl, 10 mmol/L) was added. The solution was incubated at room temperature for 30 min. The labeled DNA was purified over the Sephadex G25 column with saline, the fractions were collected to detect the radioactivity and absorbance at 260 nm, and the labeling efficiency was then assayed.

Ten micrograms of MAG_3-antisense oligonucleotide were radiolabeled, added to a reverse-phase Sep-Pak C18 column (Waters), and then eluted with acetonitrile solution (30% in ammonium acetate, 0.1 mol/L). The radioactivities and absorbance at 260 nm were detected to identify and quantitate the peak fractions. The radioactivity of the Sep-Pak column was also calculated for the radiochemical purity assessment.

To study in vitro stability, the ^{99m}Tc-MAG_3-antisense oligonucleotide was incubated in phosphate-buffered saline (PBS) and fresh human serum at a concentration of 1.2 μg/mL at 37°C, with aliquots removed at 30 min and 120 min for reverse-phase Sep-Pak C18 column analysis.

After the ^{99m}Tc-MAG_3-antisense oligonucleotide had been incubated with the unlabeled sense DNA for 60 min at 37°C, aliquots were removed for reverse-phase Sep-Pak C18 column chromatography.

VSMC Culture

Sprague–Dawley rats (mean body weight, 150 g) were obtained from the Experimental Animal Center of Tongji Medical College, Huazhong University of Science and Technology, Wuhan, China. Rat VSMCs were separated from aorta and cultured by an explant method (*21*). The culture medium was Dulbecco's modified Eagle medium (DMEM) (Gibco BRL Products) with L-glutamine, 2 mmol/L; sodium bicarbonate, 1.5 mg/L; nonessential amino acids, 0.1 mmol/L; and sodium pyruvate, 1.2 mmol/L, supplemented with 20% fetal bovine serum (FBS) and penicillin–streptomycin, 100 mg/mL (Gibco). Cells were maintained as monolayers in a humidified 5% carbon dioxide atmosphere. The cells between passage 4 and 12 were used.

The methods used for the investigation of cell uptake and efflux were as in the previous study (*19*). In brief, for uptake studies, the cells were trypsinized at 80%–90% confluence with 0.25% trypsin/0.02% EDTA and then suspended in DMEM with 10% FBS at a density of 1–2 × 10^5 cells/mL. The cells were seeded to the wells of 24-well flat-bottomed plates at 1 mL per well and incubated at 37°C in 5% carbon dioxide for 24 h to permit adherence and growth. The medium was then changed to either DMEM with 10% FBS to maintain the cells or DMEM without FBS to slow the cell growth, after which the cells were cultured further for another 24 h. Thus, the cells in the 2 different mediums were coaxed into 2 different phases: log and plateau. Cell growth and viability were monitored by inverted microscopy with phase contrast. Cell viability was detected by trypan blue exclusion.

Radiolabeled DNAs were dissolved in DMEM with 10% FBS and 0.5% FBS at a concentration of 30 ng/mL; 2 medium types were thereby prepared to be used in conjunction with the VSMCs in log and plateau phases, respectively. After the VSMC growth medium had been withdrawn, the respective DNAs were added at 1 mL per well in quadruplet. The time of addition (4, 3, 2, 1.5, 1, 0.5, and 0 h) was staggered such that the samples could be

harvested at the same time point. At harvesting, the radioactive medium was aspirated and each well was then rinsed with 1 mL of PBS. The medium and rinse were combined, and the cells were then lysed with 1 mL of 0.2N sodium hydroxide and 1% sodium dodecyl sulfate. The well contents were collected into additional counting tubes along with 1 mL of the same lysate solution, to be used as a rinse. The tubes were counted in an automatic NaI(Tl) well counter.

The efflux of radioactivity from cells previously incubated with ^{99m}Tc-labeled DNA was investigated. For the cells in log phase, multiple wells each received a total of 30 ng of radiolabeled DNA in 1 mL of solution and the cells were incubated for 1.5 h in the usual manner to maximize cell accumulation. For the cells in plateau phase, the same amounts of radiolabeled DNA and cells were incubated for 1 h to maximize cell accumulation. The medium was then replaced by medium that had no radiolabeled DNA, and cells were reincubated periodically thereafter for the next 4 h. At each time point (0, 30, 60, 120, 180, and 240 min), the medium was collected and combined with 2 mL of PBS rinse. At the end of the 4 h, the cells were harvested after rinsing. Radioactivity in each sample of medium plus wash and of the cells themselves was then determined. Cell-associated radioactivity, which indicated the retention rate, was calculated and plotted against time to obtain the efflux curve.

PCNA mRNA Expression

The ^{99m}Tc-MAG$_3$-antisense oligonucleotide and ^{99m}Tc-MAG$_3$-sense oligonucleotide were dissolved in DMEM with 10% FBS at a concentration of 5 μmol/L. The VSMCs were trypsinized at 90% confluence using 0.25% trypsin/0.02% EDTA and then suspended in DMEM with 10% FBS for an incubation period of 24 h. Then, the media were changed to DMEM with ^{99m}Tc-MAG$_3$-antisense oligonucleotide, ^{99m}Tc-MAG$_3$-sense oligonucleotide, and 10% fresh FBS, and the cells were cultured for another 48 h. Total cellular RNA was extracted from the VSMCs by TRIzol reagent (Molecular Research Center, Inc.). Reverse-transcriptase polymerase chain reaction (RT-PCR) was performed with the OneStep RT-PCR Kit (TaKaRa Bio Inc.). For reverse transcription, 1 μg of total RNA were subjected to reverse transcription primed by oligodeoxythymidine with avian myeloblastosis virus reverse transcriptase according to the recommendations of the manufacturer in a total volume of 20 μL. One microliter of a 1-in-10 dilution of complementary DNA (cDNA) was subjected to PCR using Taq DNA polymerase. To ensure analysis of PCR products in the log phase of amplification, several parallel reactions with increasing cycle numbers were performed. As an internal control for cDNA synthesis, the housekeeping gene glyceraldehyde 3-phosphate dehydrogenase (GAPDH) was amplified. PCR conditions were as follows: a hot start after 2 min at 94°C; 34 cycles consisting of denaturing for 30 s at 94°C, annealing for 30 s at 55°C, and elongation for 60 s at 72°C; and a final extension period of 6 min at 72°C. Primer sequences were as follows: PCNA, 5′ACTCTGCGCTCCGAAGG3′ (forward), 5′TCTCCAATTAGGCTAAG3′ (reverse), 274-bp predicted product size; GAPDH, 5′ACCACAGTCCATGCCATCAC3′ (forward), 5′TCCACCACCCTGTTGCTGTA3′ (reverse), 516 bp. Each PCR product was size-fractionated by 2% agarose gel electrophoresis. The gel was stained with ethidium bromide (1 μg/mL), visualized using an ultraviolet transilluminator, and photographed. The density of each PCR band was measured and analyzed by video documentation system software (ImageMaster; Pharmacia Biotech), and the amount of mRNA products for PCNA was expressed as the ratio to GAPDH mRNA product, which served as the internal control.

RESULTS

Coupling and Radiolabeling

The ^{99m}Tc radiolabeling efficiency of MAG$_3$-antisense oligonucleotide was significantly higher in the group with chelator than in the control group lacking the chelator (60.1% ± 3.02% vs. 5% ± 2.1%, $P < 0.001$, $n = 5$), indicating that radiolabeling was mediated mainly by the chelator. For ^{99m}Tc-MAG$_3$-antisense oligonucleotide, the specific activity was 1,960 kBq/μg, and the radiochemical purity was above 95% after purification. After the MAG$_3$-antisense oligonucleotide and unconjugated antisense oligonucleotide had been radiolabeled by ^{99m}Tc, 2 peaks were found in all the ultraviolet absorption profiles, but only the first ultraviolet absorption peak of the MAG$_3$-antisense oligonucleotide indicated radioactivity (Fig. 1).

Stability in Serum and Hybridization Ability

After ^{99m}Tc-MAG$_3$-antisense oligonucleotide had been incubated in fresh human serum and PBS at 1.2 μg/mL, the radioactivity peak showed no shift to early or late fractions (Fig. 2); however, the peak appeared late after ^{99m}Tc-MAG$_3$-antisense oligonucleotide had been incubated with sense oligonucleotide. The recoveries of DNA as shown in Figure 2 approached 80% at one time, but the typical recovery was about 70% (SD = 5.5, $n = 5$).

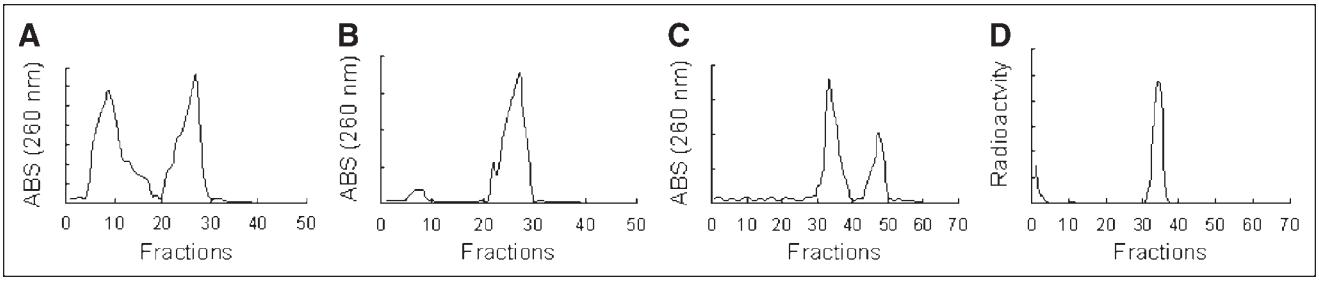

FIGURE 1. (A–C) Ultraviolet absorption (ABS) profiles of fractions obtained by Sephadex G-25 chromatography (MAG$_3$-DNA [A] and DNA [B]) and reverse-phase Sep-Pak C18 chromatography (MAG$_3$-DNA [C]) after radiolabeling. (D) Radiochromatogram obtained by Sep-Pak C18 chromatography of MAG$_3$-DNA after radiolabeling. The traces shown in A, B, and C contain 2 peaks. The trace shown in D reveals that only the first peak of C indicates radioactivity. Recovery was typically about 70% (SD = 5.5; $n = 5$).

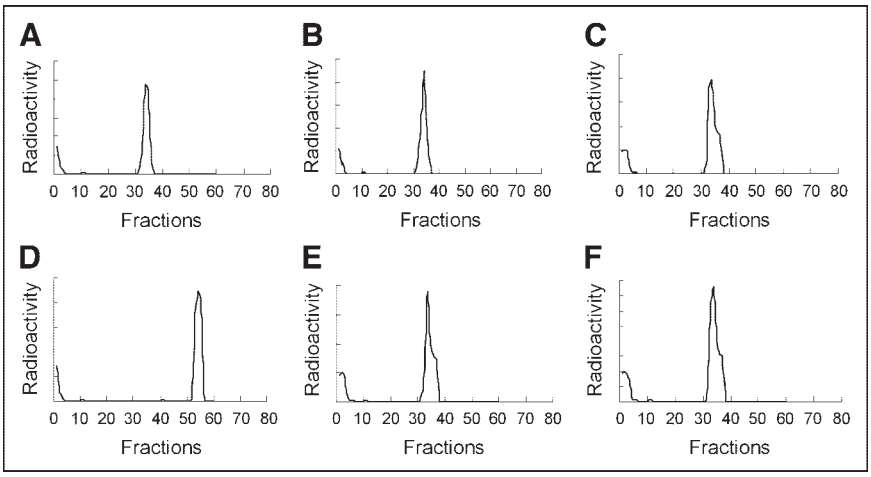

FIGURE 2. Radiochromatograms obtained by reverse-phase Sep-Pak C18 analysis of ^{99m}Tc-MAG$_3$-antisense oligonucleotide before and after incubation with PBS, fresh serum, and complementary chain. (A) Radioactivity of fractions after Sep-Pak C18 chromatography before radiolabeled DNA was incubated with serum and PBS. (D) Radioactivity of fractions after DNA was incubated with complement chain, in which radioactivity peak appeared late. (B and E) Radioactivity of fractions after DNA was incubated with PBS for 30 and 120 min. (C and F) Radioactivity after incubation with fresh serum for 30 and 120 min.

Cell Uptake of Radiolabeled DNA

By Trypan blue exclusion, the viability of cells in all phases of this study was estimated to be no less than 95%.

Figure 3 represents cell-associated radioactivity in cultured VSMCs for ^{99m}Tc-MAG$_3$-sense oligonucleotide and ^{99m}Tc-MAG$_3$-antisense oligonucleotide. For the cells in log phase, the highest accumulation of both antisense and sense DNA occurred at 90 min, with peak values of 15.2% ± 0.58% and 5.6% ± 0.42%, respectively ($P < 0.05$, $n = 4$). For the cells in plateau phase, the highest accumulation occurred at 60 min, with no significant difference between the 2 DNAs (1.54% ± 0.26% and 1.52% ± 0.28%, respectively, $P > 0.05$, $n = 4$). Uptake of the ^{99m}Tc-MAG$_3$-antisense oligonucleotide was much higher in cells in log phase than in cells in plateau phase (15.2% ± 0.58% and 1.54% ± 0.26%, respectively, $P < 0.05$, $n = 4$).

Cellular Efflux of Radiolabeled DNA

Figure 4 shows the percentage of ^{99m}Tc radioactivity leaving cells during the 4 h after washing and replacement of the medium. Before this point, the cells in log and plateau phases had been incubated for 90 min and 60 min, respectively. At 4 h, a statistically significant difference in efflux was observed between ^{99m}Tc-MAG$_3$-antisense oligonucleotide and ^{99m}Tc-MAG$_3$-antisense oligonucleotide in cells in log phase, and no difference was observed between the 2 DNAs in cells in plateau phase. For the ^{99m}Tc-MAG$_3$-antisense oligonucleotide, the efflux was slower in cells in log phase than in cells in plateau phase.

Effect of ^{99m}Tc-Labeled PCNA Antisense Oligonucleotide on mRNA Expression

After 48 h, a significant ($P < 0.01$) decrease of PCNA mRNA was observed in cells treated with ^{99m}Tc-MAG$_3$-antisense oligonucleotide, compared with those treated with ^{99m}Tc-MAG$_3$-sense oligonucleotide or 10% FBS, and no significant difference was observed between the cells

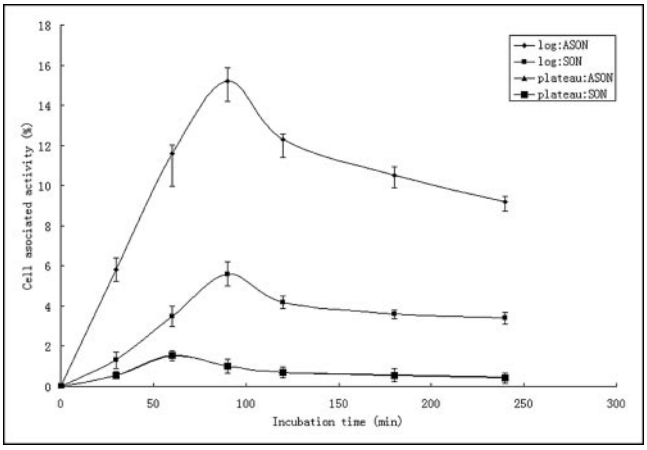

FIGURE 3. Cell-associated radioactivity in cultured VSMCs for ^{99m}Tc-labeled sense and antisense DNA. For cells in log phase, antisense DNA shows significantly higher cell accumulation at all time points than does sense DNA; highest accumulation of both sense and antisense DNA occurs at 90 min. For cells in plateau phase, highest accumulation occurs at 60 min.

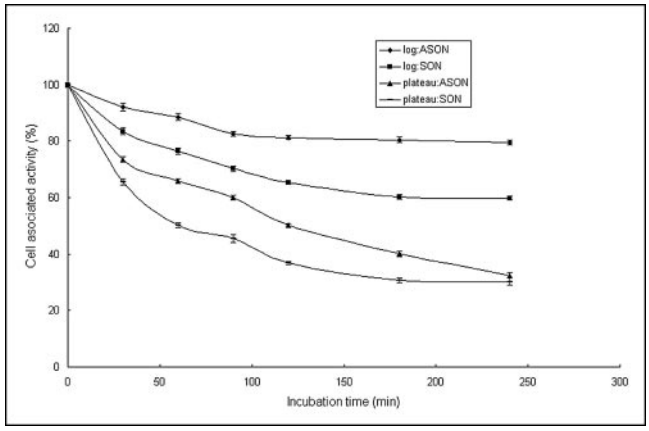

FIGURE 4. Efflux of ^{99m}Tc-MAG$_3$-DNA over time from VSMCs in log and plateau phases. Retention of antisense oligonucleotide is higher than that of sense oligonucleotide at many time points both in cells in log phase and in cells in plateau phase. The 2 oligonucleotides (antisense oligonucleotide and sense oligonucleotide) show greater efflux rate in cells in plateau phase than in cells in log phase.

treated with ^{99m}Tc-MAG$_3$-sense oligonucleotide and 10% FBS (Fig. 5).

DISCUSSION

Coronary artery disease remains one of the greatest health problems in developed countries. Many advances have been made in the treatment of atherosclerosis; however, morbidity and mortality remain significant, as do treatment failures and recurrence (*22*).

Many different techniques for imaging atherosclerosis aid both in diagnosis and in guiding future management; these techniques can be categorized as invasive or noninvasive. Invasive imaging techniques include x-ray angiography, intravascular ultrasound, angioscopy, and intravascular thermography (*23–25*). These catheter-based techniques, especially intravascular ultrasound and thermography, can provide important information on the composition of individual plaques, but their invasive nature limits their use to only a few patients with well-defined diseases. Noninvasive imaging techniques include B-mode duplex ultrasound, CT, MRI, and functional imaging techniques such as SPECT and PET. Both CT and MRI can provide more than simple angiographic data. In particular, electron-beam CT can accurately quantify coronary calcium, but it cannot identify other components in the early lesions. Recent studies have shown that MRI is capable of discriminating compositions in atherosclerotic lesions; however, considerably more work is required to overcome problems caused by artifacts, poor resolution, and interpretation of signal heterogeneity before MRI can realistically be used to assess coronary artery plaque composition.

Most of the techniques described so far, with the possible exception of thermography, have been aimed at providing anatomic detail on plaque size and, to a limited extent, composition. However, none is able to provide information on cell biologic events. Several radiolabeled tracers have been developed that can bind to or be taken up by constituents of atherosclerotic plaque or associated surface thrombus, such that 2-dimensional tomographic and 3-dimensional reconstructive images can be extrapolated from emitted γ-rays, usually by means of SPECT, or positrons by PET. The radiotracers for imaging atherosclerosis include ^{99m}Tc-low-density lipoprotein, ^{99m}Tc-oxidized low-density lipoprotein, radiolabeled antibodies directed against cells and antigens present in atherosclerotic lesions, radiolabeled peptides, ^{99m}Tc-annexin V, and ^{18}F-FDG (*26–32*). In animal experiments, some of the radiotracers can provide high target (atherosclerotic plaque)-to-background (blood pool) ratios, indicating the atherosclerotic lesions clearly.

It has been proven that a series of molecular pathways of disease development and progression are common both to atherosclerosis and to cancer (*33*) and that they share some biologic characteristics: the abnormal proliferation of cells and high expression of some oncogene and cell-cycle proteins such as c-*myc*, c-*fos*, and PCNA. The in vivo gene imaging studies using antisense probe have proven this method a feasible option in detecting tumor tissue (*12–17*). Recently, Qin et al. reported that the radiolabeled antisense probe to c-*myc* oncogene could indicate the atherosclerotic plaque in rabbits (*18*).

Animal experiments and immunochemistry findings on human atherosclerotic and restenotic tissue have suggested that vascular cell proliferation prevails at the onset of atherosclerosis and restenosis. Among excessively proliferating cells, VSMCs are the preponderant proliferating cell type in the vasculature and normally are latent cells in the G0 phase of the cell cycle. VSMC proliferation in animal experiments and human atherosclerotic and restenotic tissue is associated with a temporally and spatially coordinated expression of cell cycle–dependent kinases and cyclins, suggesting that induction of positive cell-cycle control genes is a hallmark of vascular proliferative disease (*34,35*).

The pathophysiologic theory about atherosclerosis reveals that the process of atherosclerosis is a complicated

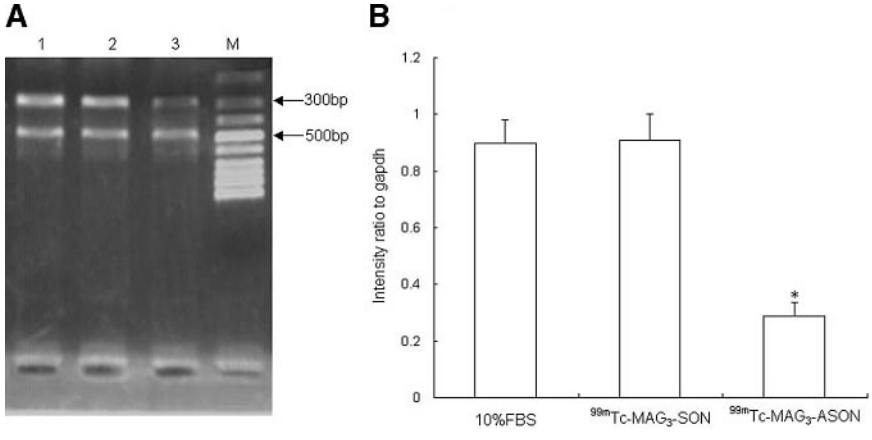

FIGURE 5. Effect of ^{99m}Tc-MAG$_3$-antisense oligonucleotide and ^{99m}Tc-MAG$_3$-sense oligonucleotide on PCNA mRNA expression. VSMCs were cultured with 5 μmol/L concentrations of radiolabeled antisense oligonucleotide, sense oligonucleotide, and FBS for 48 h, and RNA was extracted and checked for purity. After reverse transcription, RNA–cDNA hybrids were used as templates for RT-PCR. (A) Lane 1, cells incubated with 10% FBS; lane 2, cells treated with ^{99m}Tc-MAG$_3$-sense oligonucleotide; lane 3, cells treated with ^{99m}Tc-MAG$_3$-antisense oligonucleotide; lane M, DNA standard marker. (B) Intensity ratio of each band to internal control (GAPDH mRNA). *Significantly ($P < 0.01$) lower quantity of PCNA mRNA in cells treated with labeled antisense oligonucleotide than in cells treated with 10% FBS.

system comprising a network of different cells, growth factors, and cytokines. The accelerating or inhibiting effect will amass at the boundary of cell cycle G0/S, with the ultimate effect reflected in the proliferation of VSMCs.

Because PCNA is the cofactor of DNA polymerase δ and functions in provoking cells in G0 phase to enter S phase and accelerating DNA synthesis, its expression can directly indicate the extent of cell proliferation. In clinical practice, the immunochemistry stain on PCNA is always used to evaluate the extent to which abnormally proliferating tissues are malignant (*36–39*).

In the research of Speir and Epstein (*40*), 4 sequences of PCNA were modified and the antisense oligodeoxyribonucleotide inhibited the proliferation of smooth muscle cells by 50% and decreased DNA replication. Western blotting and immunohistology revealed that the antisense oligodeoxyribonucleotide could decrease the expression of PCNA, proving that PCNA is essential in the smooth muscle cell cycle, division process, and DNA replication.

Although PCNA is not the biomarker appearing at the beginning of pathophysiologic alteration, it can directly indicate the early proliferation of VSMCs that prevails at the onset of atherogenesis and restenosis. One can infer that use of PCNA detection to reflect the early proliferative changes of atherosclerosis and restenosis will be more feasible.

Having this information, we tried to apply PCNA to the study of atherosclerosis and restenosis using early gene imaging. In this study, 2 oligonucleotides with 18 bases were reproduced; one was the antisense oligonucleotide complementary to the 5′ initiation codon regions of PCNA, and the other was the respective sense strand. The antisense oligonucleotide was conjugated with the bifunctional chelator MAG_3, which was used to radiolabel antisense oligonucleotide with the γ-emitting metal ^{99m}Tc. The labeling efficiency of MAG_3-antisense oligonucleotide was more than 60%, and the radiochemistry purity after purification was up to 95%, which is close to the percentage previously reported (*19,20*). The ^{99m}Tc-MAG_3-antisense oligonucleotide was stable in serum after 60 min and maintained its hybridization ability with sense oligonucleotide. In the VSMCs in log phase, ^{99m}Tc-MAG_3-antisense oligonucleotide can be taken up significantly. The accumulation was much higher than that in the VSMCs in plateau phase, and the efflux was slower in the proliferating cells.

Many factors, such as membrane permeability, steric hindrance, and electric charge on the molecules, can affect the accumulation of the antisense probes at the aimed-for sequence on the whole DNA or mRNA strand in cells. In this study, ^{99m}Tc-MAG_3-antisense oligonucleotide could hybridize to the synthesized 18mer sense oligonucleotide after incubation, but this finding did not prove that the antisense probe could still hybridize to the sequence on the whole PCNA mRNA in proliferating VSMCs. To solve this problem, RT-PCR was performed to assay the mRNA level after proliferating cells had been incubated with the antisense probe at a high concentration of 5 μmol/L. The results revealed that ^{99m}Tc-MAG_3-antisense oligonucleotide could decrease the mRNA level significantly, compared with ^{99m}Tc-MAG_3-sense oligonucleotide, further proving that conjugation and radiolabeling did not affect the hybridization ability of the antisense oligonucleotide.

In this study, antisense PCNA probe accumulated in proliferating VSMCs, the main component of atherosclerotic plaque, and the ^{99m}Tc-MAG_3-antisense oligonucleotide was still able to hybridize to the candidate gene in proliferating VSMCs after radiolabeling, thereby proving that we can further use the ^{99m}Tc-MAG_3-antisense oligonucleotide (PCNA) for in vivo imaging of atherosclerotic plaque and restenosis. Because PCNA is the marker directly indicating cell proliferation, it can also be used for in vivo imaging of proliferating tumors. If the antisense probe can display lesions in the case of animals, we will come closer to acquiring a new method to investigate proliferative diseases early and noninvasively.

A limitation of this study was that the antisense probe accumulates in all proliferating cells, including the abnormally proliferating VSMCs and tumor cells. Further research on targeted delivery of the antisense probe is therefore needed.

CONCLUSION

This in vitro study in VSMCs provided evidence that the ^{99m}Tc-labeled antisense oligonucleotide to PCNA can be used for in vivo imaging of atherosclerotic plaque and restenosis in further study.

ACKNOWLEDGMENTS

Professor Donald J. Hnatowich (University of Massachusetts Medical School) is gratefully acknowledged for providing MAG_3-NHS for conjugation. This study was supported by the National Natural Science Foundation of China (NSFC 30070310).

REFERENCES

1. Zamecnik PC, Stephenson ML. Inhibition of Rous sarcoma virus replication and cell transformation by a specific oligodeoxynucleotide. *Proc Natl Acad Sci.* 1978;75:280–284.
2. Abaza MS, Al-Attiyah RJ, Al-Saffar AM, et al. Antisense oligodeoxynucleotide directed against c-myb has anticancer activity and potentiates the antiproliferative effect of conventional anticancer drugs acting by different mechanisms in human colorectal cancer cells. *Tumour Biol.* 2003;24:241–257.
3. Crooke ST. Molecular mechanisms of action of antisense drugs. *Biochim Biophys Acta.* 1999;1489:31–44.
4. Joshi PJ, Fisher TS, Prasad VR. Anti-HIV inhibitors based on nucleic acids: emergence of aptamers as potent antivirals. *Curr Drug Targets Infect Disord.* 2003;3:383–400.
5. Clawson GA, Miranda GQ, Sivarajah A, et al. Inhibition of papilloma progression by antisense oligonucleotides targeted to HPV11 E6/E7 RNA. *Gene Ther.* 2004;11:1331–1341.
6. Fukuda N, Furuya R, Kishioka H, et al. Effects of antisense peptide nucleic acid to platelet-derived growth factor A-chain on growth of vascular smooth muscle cells. *J Cardiovasc Pharmacol.* 2003;42:224–231.
7. Suzuki J, Isobe M, Morishita R, et al. Antisense Bcl-x oligonucleotide induces apoptosis and prevents arterial neointimal formation in murine cardiac allografts. *Cardiovasc Res.* 2000;45:783–787.

8. Suzuki J, Isobe M, Morishita R, et al. Prevention of cardiac allograft arteriosclerosis using antisense proliferating-cell nuclear antigen oligonucleotide. *Transplantation.* 200070:398–400.
9. Kipshidze NN, Kim HS, Iversen P, et al. Intramural coronary delivery of advanced antisense oligonucleotides reduces neointimal formation in the porcine stent restenosis model. *J Am Coll Cardiol*. 2002;39:1686–1691.
10. Freedman SB. Clinical trials of gene therapy for atherosclerotic cardiovascular disease. *Curr Opin Lipidol.* 2002;13:653–661.
11. Hudziak RM, Summerton J, Weller DD, et al. Antiproliferative effects of steric blocking phosphorodiamidate morpholino antisense agents directed against c-myc. *Antisense Nucleic Acid Drug Dev.* 2000;10:163–176.
12. Roivainen A, Tolvanen T, Salomaki S, et al. ^{68}Ga-labeled oligonucleotides for in vivo imaging with PET. *J Nucl Med.* 2004;45:347–355.
13. Tavitian B. In vivo imaging with oligonucleotides for diagnosis and drug development. *Gut.* 2003;52:iv40–iv47.
14. Tian X, Aruva MR, Rao PS, et al. Imaging oncogene expression. *Ann N Y Acad Sci.* 2003;1002:165–188.
15. Gallazzi F, Wang Y, Jia F, et al. Synthesis of radiometal-labeled and fluorescent cell-permeating peptide-PNA conjugates for targeting the bcl-2 proto-oncogene. *Bioconjug Chem.* 2003;14:1083–1095.
16. McCaffrey AP, Meuse L, Karimi M, et al. A potent and specific morpholino antisense inhibitor of hepatitis C translation in mice. *Hepatology.* 2003;38:503–508.
17. Rao PS, Tian X, Qin W, et al. ^{99m}Tc-peptide-peptide nucleic acid probes for imaging oncogene mRNA in tumors. *Nucl Med Commun.* 2003;24:857–863.
18. Qin G, Zhang Y, Cao W, et al. Molecular imaging of atherosclerotic plaques with technetium-99m-labelled antisense oligonucleotides. *Eur J Nucl Med Mol Imaging.* 2005;32:6–14.
19. Winnard P Jr, Chang F, Rusckowski M, et al. Preparation and use of NHS-MAG_3 for technetium-99m labeling of DNA. *Nucl Med Biol.* 1997;24:425–432.
20. Zhang YM, Liu N, Zhu ZH, et al. Influence of different chelators (HYNIC, MAG_3 and DTPA) on tumor cell accumulation and mouse biodistribution of technetium-99m labeled to antisense DNA. *Eur J Nucl Med.* 2000;72:1700–1707.
21. Lawson C, Ainsworth ME, McCormack AM, et al. Effects of cross-linking ICAM-1 on the surface of human vascular smooth muscle cells: induction of VCAM-1 but no proliferation. *Cardiovasc Res.* 2001;50:547–555.
22. Selkirk SM. Gene therapy in clinical medicine. *Postgrad Med J.* 2004;80:560–570.
23. Dinsmore R. Imaging techniques in carotid and peripheral vascular disease. In: Fuster V, ed. *Syndromes of Atherosclerosis: Correlations of Clinical Imaging and Pathology.* Armonk, NY: Futura Publishing Co., Inc.; 1996:277–289.
24. von Birgelen C, Slager CJ, Di Mario C, et al. Volumetric intracoronary ultrasound: a new maximum confidence approach for the quantitative assessment of progression-regression of atherosclerosis? *Atherosclerosis.* 1995;118:S103–S113.
25. den Heijer P, Foley DP, Hillege HL, et al. The "Ermenonville" classification of observations at coronary angioscopy: evaluation of intra- and inter-observer agreement—European Working Group on Coronary Angioscopy. *Eur Heart J.* 1994;15:815–822.
26. Iuliano L, Signore A, Vallabajosula S, et al. Preparation and biodistribution of 99m-technetium labelled oxidized LDL in man. *Atherosclerosis.* 1996;126:131–141.
27. Tsimikas S, Palinski W, Halpern SE, et al. Radiolabeled MDA2, an oxidation-specific, monoclonal antibody, identifies native atherosclerotic lesions in vivo. *J Nucl Cardiol.* 1999;6:41–53.
28. Hardoff R, Braegelmann F, Zanzonico P, et al. External imaging of atherosclerosis in rabbits using an ^{123}I-labeled synthetic peptide fragment. *J Clin Pharmacol.*1993;33:1039–1047.
29. Carrio I, Pieri PL, Narula J, et al. Noninvasive localization of human atherosclerotic lesions with indium 111-labeled monoclonal Z2D3 antibody specific for proliferating smooth muscle cells. *J Nucl Cardiol.* 1998;5:551–557.
30. Stratton JR, Dewhurst TA, Kasina S, et al. Selective uptake of radiolabeled annexin V on acute porcine left atrial thrombi. *Circulation.* 1995;92:3113–3121.
31. Yun M, Jang S, Cucchiara A, et al. ^{18}F-FDG uptake in the large arteries: a correlation study with the atherogenic risk factors. *Semin Nucl Med.* 2002;32:70–76.
32. Rudd JH, Warburton EA, Fryer TD, et al. Imaging atherosclerotic plaque inflammation with [^{18}F]-fluorodeoxyglucose positron emission tomography. *Circulation.* 2002;105:2708–2711.
33. Lavezzi AM, Milei J, Grana DR, et al. Expression of c-fos, p53 and PCNA in the unstable atherosclerotic carotid plaque. *Int J Cardiol.* 2003;92:59–63.
34. Wei GL, Krasinski K, Kearney M, et al. Temporally and spatially coordinated expression of cell cycle regulatory factors after angioplasty. *Circ Res.* 1997;80:418–426.
35. Ihling C, Technau K, Gross V, et al. Concordant upregulation of type II-TGF-beta-receptor, the cyclin-dependent kinases inhibitor P27Kip1 and cyclin E in human atherosclerotic tissue: implications for lesion cellularity. *Atherosclerosis.* 1999;144:7–14.
36. Shen LJ, Zhang HX, Zhang ZJ, et al. Detection of HBV, PCNA and GST-pi in hepatocellular carcinoma and chronic liver disease. *World J Gastroenterol.* 2003;9:459–462.
37. Shang S, Takai N, Nishida M, et al. CaMKIV expression is associated with clinical stage and PCNA-labeling index in endometrial carcinoma. *Int J Mol Med.* 2003;11:181–186.
38. Jorge O, Parasi AS, Manioudaki HS, et al. Prognostic impact of DNA ploidy pattern, S-phage fraction (SPF), and proliferating cell nuclear antigene (PCNA) in patients with primary gastric lymphoma. *J Surg Oncol.* 2003;82:247–255.
39. Kushlinskii NE, Orinovskii MB, Gurevich LE, et al. Expression of biomolecular markers (Ki-67, PCNA, Bcl-2, BAX, BclX, VEGF) in breast tumors. *Bull Exp Biol Med.* 2004;137:182–185.
40. Speir E, Epstein SE. Inhibition of smooth muscle cell proliferation by an antisense oligodeoxynucleotide targeting the messenger RNA encoding proliferating cell nuclear antigen. *Circulation.* 1992;86:538–547.